Real-time wavelet-transform spectrum analyzer for the investigation of $1/f^\alpha$ noise

Doriano Brogioli and Alberto Vailati
Dipartimento di Fisica and Istituto Nazionale per la Fisica della Materia, Università di Milano, via Celoria 16, 20133 Milano, Italy

A wavelet transform spectrum analyzer operating in real time within the frequency range $3 \times 10^{-5} - 1.3 \times 10^5$Hz has been implemented on a low-cost Digital Signal Processing board operating at 150MHz. The wavelet decomposition of the signal allows to efficiently process non-stationary signals dominated by large amplitude events fairly well localized in time, thus providing the natural tool to analyze processes characterized by $1/f^\alpha$ power spectrum. The parallel architecture of the DSP allows the real-time processing of the wavelet transform of the signal sampled at 0.3MHz. The bandwidth is about 220dB, almost ten decades. The power spectrum of the scattered intensity is processed in real time from the mean square value of the wavelet coefficients within each frequency band. The performances of the spectrum analyzer have been investigated by performing Dynamic Light Scattering experiments on colloidal suspensions and by comparing the measured spectra with the correlation functions data obtained with a traditional multi tau correlator. In order to asses the potentialities of the spectrum analyzer in the investigation of processes involving a wide range of timescales, we have performed measurements on a model system where fluctuations in the scattered intensities are generated by the number fluctuations in a dilute colloidal suspension illuminated by a wide beam. This system is characterized by a power-law spectrum with exponent $-3/2$ in the scattered intensity fluctuations. The spectrum analyzer allows to recover the power spectrum with a dynamic range spanning about 8 decades. The advantages of wavelet analysis versus correlation analysis in the investigation of processes characterized by a wide distribution of time scales and non-stationary processes are briefly discussed.

PACS numbers: 07.50.Qx, 07.60.Rd, 02.70.Rr, 05.40.Ca, 05.45.Df

I. INTRODUCTION

The investigation of random processes characterized by a wide range of timescales is becoming increasingly important in many experimental fields ranging from the investigation of earthquakes in earth-science, to turbulence in fluids, or the price fluctuations in financial markets [1, 2, 3, 4]. In particular, many random processes exhibit a scale invariant structure. The self-similarity of the signal is reflected in the power law behavior of the power spectrum, which lacks characteristic time scales.

Traditional spectral decomposition techniques often fail when applied to a self similar signal. This is due to the fact that such a signal is typically the superposition of bursts occurring at many different timescales. Although rare, long bursts having a very large amplitude provide much of the energy content of the signal, while short bursts with small amplitude, although very frequent, give small contribution to the energy of the signal. The energy is therefore fairly well localized in time and the signal is non-stationary. This localization prevents Fourier Analisys to work as an effective tool for this kind of signal.

However, a scale invariant signal can be efficiently analyzed by using the renormalization group approach devised in statistical physics to describe systems at a critical point [5]. The self similar system goes through a consecutive sequence of coarse grainings which generate a new signal with statistical properties similar to those of the original one.

In practice the renormalization group analisys of a signal is achieved by using the wavelet transform technique. Basically the signal is convolved with a chosen mother wavelet function. The mother wavelet consists in a truncated wave packet with central frequency ω and bandwidth Γ, localized at time t, with length $l \propto 1/\Gamma$. The mean square amplitude of this component provides the power spectral amplitude of the signal in the frequency range $(\omega - \Gamma, \omega + \Gamma)$. An in-quadrature component of the signal is also simultaneously processed to recover the discarded lower frequency component, representing the coarse grained signal. The mother wavelet is then rescaled on a larger scale and the process iterated.

In this paper we describe a real-time wavelet transform spectrum analyzer (WTSA) working in the frequency range $3 \times 10^{-5} - 1.3 \times 10^5$Hz. The spectrum analyzer is built around a Texas Instruments C6711 DSP Starter Kit (DSK). This board incorporates a C6711 DSP running at 150MHz together with a parallel port to communicate with a Personal computer and various connectors to interface the board to the real world. Solutions based on wavelet analysis by means of the post processing on a dedicated personal computer of the digitized signal have recently been proposed [6, 7]. The highly parallel processing architecture of the DSP allows the real-time processing of the wavelet transform of the signal sampled at 0.3MHz. The bandwidth spans almost ten decades.

We will present applications to Dynamic Light Scattering (DLS) from colloidal suspensions and compare the results obtained with the WTSA with the correlation function obtained with a traditional multi tau correlator. Dynamic Light Scattering has been used very extensively to investigate stochastic fluctuations in the intensity of the

light scattered by suspended particles undergoing brownian motion, aggregation processes, gelation processes, critical dynamics [8, 9, 10]. In recent times, processes characterized by a wide distribution of relaxation times, often leading to stretched-exponential decay of the autocorrelation function, have attracted much interest (see Refs. [11, 12] and references therein). The development of log-scale correlators has allowed the investigation of processes extending from about 100ns up to hours. However, large time lags require very long acquisitions times to get good statistical accuracy in the correlation tails.

The wavelet analisys of the fluctuations in the intensity of the scattered light provides higher accuracy in shorter times when compared to DLS when non-stationary self similar signals are processed. This is due to the fact that the localized wavelets used to process the signal are very efficient in isolating the well localized features of a self-similar signal, and this provides a shorter convergence time of the processing to get results with a chosen statistical accuracy.

To asses the potentialities of the WTSA in investigating time-scale invariant systems we have devised a simple model system giving rise to a power-law spectrum with exponent $-3/2$. This system is made up by strongly diluted brownian particles diffusing within a large sampling volume. We show that the WTSA is able to measure the power spectrum within a dynamic range as large as 8 decades. We also show that the WTSA requires a measurement time roughly 100 times smaller than that needed by a correlator to get the same statistical accuracy at large lag times.

II. WAVELET ANALYSIS

The wavelet analisys of signals is becoming increasingly popular within the scientific community. With respect to traditional Fourier decomposition techniques, wavelet analisys allows to characterize signals having a large bandwidth by using a small number of coefficients.

Basically, instead of decomposing the signals into armonic oscillations as in Fourier analisys, the signal gets decomposed into the superposition of wave packets (WP). The WP are localized both in time and in frequency. These wave packets are obtained by rescaling a chosen Mother Wavelet (MW) $\Psi(t)$ with a proper scale s so as to obtain a wavelet function $\varphi_{t_0,s}(t) = \Psi\left(\frac{t-t_0}{s}\right)$. The wavelets exhibit the same functional form of the MW, but are centered around time t_0 and their bandwidth is a factor s larger than that of the MW. Therefore, if the signal has a bump at time t with a certain duration Δt the wavelet decomposition will likely give rise to a wave packet localized at t with a scale s proportional to the duration of the bump. This allows a very efficient decomposition of spiky signals and non-stationary signals in general. In practice the wavelet analysis is usually performed by using the popular Discrete Wavelet Transform (DWT) algorithm [13]. To apply this algorithm, one starts with a sampled discrete signal y_n^0 made up by 2^N samplings, where N is an integer. The signal undergoes successive coarse grainings and band-pass filterings by convolution with a chosen wavelet set. The scale s of the wavelets used during the coarse grainings changes by a factor 2 at each step, so that the scaling of the signal at the k-th step is given by $s_k = s_0 2^k$. On the contrary, the number of samplings in the coarse grained signal decreases as $2^N/2^k$. Therefore, as the scale increases due to the successive scale doublings, the resolution in the temporal localization of the wavelet decreases accordingly. In the following we will give a brief and more rigorous overview on how the power spectrum is processed from the sampled signal.

Consider a discrete signal y_n^0 sampled at a given sample frequency f_s. According to Nyquist theorem the higher angular frequency it contains is $\omega_0 = \pi f_s$, that corresponds to the function $y_n^0 = (-1)^n$. The original signal y_n^0 is passed through a high-pass filter, giving the wavelet coefficients c_n^0, representing the high frequency details of the signal in the range $(\omega_0/2, \omega_0)$, and through a low-pass filter, giving a coarse grained signal y_n^1. Both the filters are implemented by convolving the signal with suitable filter coefficients g_n (the MW) and h_n; they are localized in n so that the only non vanishing elements are the ones with $0 \le n < M$:

$$\begin{cases} c_j^0 = \sum_n y_n^0 g_{n-2j} \\ y_j^1 = \sum_n y_n^0 h_{n-2j} \end{cases} . \tag{1}$$

Both the filtered signals c_n^0 and y_n^1 are sampled at half the original frequency f_s. The two filter coefficients h_n and g_n are such that the coarse grained signal y_n^1, along with the details c_n^0, allow to recover the whole original signal y_n^0: they are referred to as quadrature mirror filters. In the measurements we performed we used Daubechies wavelets [13].

The procedure is then iterated, using y_n^1 as the new signal; a high frequency component c_n^1 is obtained together with a coarse grained signal y_n^2, and so on. In general, the following recursion formulas apply:

$$\begin{cases} c_j^k = \sum_n y_n^k g_{n-2j} \\ y_j^{k+1} = \sum_n y_n^k h_{n-2j} \end{cases} . \tag{2}$$

At step k, the signal y_n^k is coarse grained to obtain y_n^{k+1}; the high frequency details, spanning the angular frequency range $\left(\omega_0/2^{k+1}, \omega_0/2^k\right)$ are the wavelet coefficients c_n^k.

The power spectrum of the signal can then be derived from the mean square average of the details $\left\langle \left|c_n^k\right|^2 \right\rangle_n$.

With the traditional Fourier transform, the analyzed wavelengths are discretized, due to the finiteness of the sample; the spacing between two consecutive wavenumbers is constant. Unlikely, with wavelet analysis, the spacing is exponential: the mean square amplitude of the wavelet coefficients represents the power contained in an octave.

The exponential spacing is particularly suited to measure phenomena spanning many decades in wavenumber. This feature is analogous to the multi tau analysis done by the best commercial correlators. Though the power spectrum and the correlation function are connected by the well known Wiener-Kintchine theorem, in many actual cases it is not possible to recover the power spectrum by the measurement of the correlation function. In general, the exponential spaced correlation function given by a multi-tau correlator cannot be safely Fourier transformed into the power spectrum, over many decades. Moreover, in some cases Wiener-Kintchine theorem does not apply. This is the case of some scale invariant and non-stationary signals; in Sect. V B we present an example in which the power spectrum obtained by the wavelet analysis correctly shows a power law behaviour, while a multi tau correlator seemingly says that the signal is delta correlated.

The analogy between the wavelet analysis and the multi tau correlation also includes the possibility of performing the required processing in real time, as the sample is acquired. With Fourier analysis, as the sample becomes larger, we must analyze more and more wavelengths, and this requires that all the sample is recorded and re-analyzed. On the contrary, as time goes on, the multi tau correlator averages the older samples; as a new, longer delay time is available, the correlation function is evaluated from only a few registers. This allows to extend the dynamic range in time delay over many decades, without the need to record the samples with the same, huge dynamic range. The same thing happens with the WTSA. The iterative procedure is implemented by using N, almost identical levels k. The memory needed scales as N while the time needed by the processing does not change at all, as we will show in Sect. IV; on the other hand, the frequency range scales as 2^N.

III. THE WAVELET TRANSFORM SPECTRUM ANALYZER

The spectrum analyzer is built around a Texas Instruments C6711 DSP Starter Kit (DSK), graciously provided by Texas Instruments DSP University Program.

This board incorporates a C6711 DSP running at 150MHz, together with a parallel port to communicate with a Personal computer and various connectors to interface the board to the real world. The software can be developed on a Personal Computer by using TI Code Composer Studio and then downloaded on the board. The board and the bundled software are very cheap compared to a real time correlator board, the purchase price being of the order of 300$ for educational institutions.

The core of the board is made up by a Digital Signal Processor, a single-chip programmable device including a CPU specifically suited for digital signal processing [14]. The DSP is a TMS320C6711, built by Texas Instruments, one of the fastest processors currently available. It is based on VelociTI, a high-performance, advanced very-long-instruction-word architecture, and its CPU can perform operations on double precision (64 bit) floating point numbers.

The CPU is divided into two almost identical sides; each of them includes 16 registers, one word (32 bit) long. Couples of registers can be used to represent one floating point, double precision register. Each section includes four ALUs, operating simultaneously; each ALU can perform only a given set of operations. Data paths from registers to memory and from a register in one side to an ALU in the other are also provided.

The CPU works at 150MHz. At each clock cycle, up to eight instructions are fetched, dispatched and decoded, that is, up to one instruction for each ALU. All the fixed point instructions are executed in one clock cycle; this means that the CPU can perform 1.2×10^9 instructions per second, a figure comparable to the number of MFLOPS available on a 2GHz Pentium IV processor. Some floating point instructions require more than one clock cycle to return the results (execution latency); generally, the same unit can start a new instruction after a few clock cycles (functional unit latency), before the results of the previous operations are availabe. For example, the functional unit latency of a double precision floating point multiplication is 4 clock cycles, and the execution latency is 9 clock cycles. Consider, for example, an ALU starting a multiplication at $t = 0$: at $t = 4$ clock cycles it can start a new multiplication and at $t = 9$ clock cycles the results of the first multiplication are available on the registers. Since there are two ALUs able to perform floating point multiplications, the CPU can do 60×10^6 multiplications per second, and, simultaneously, much more floating point additions, using other two ALUs. This structure requires a sophisticated, parallel programming technique, resulting in extremely fast, real time programs.

The DSP includes a two level memory [15]. The first level is composed by two 4Kbytes cache memories, L1P for the program instructions and L1D for the data. The second level, L2, is a 64Kbytes RAM, that can be configured partially as a SRAM or as a chache for an external memory. Since our program and data fit in the SRAM, we didn't use the slower external RAM and we configured all the L2 as SRAM. Reads and writes in the L1P and L1D memories are performed in four clock cycles; obviously, L2 is slower and a miss in the L1 cache results in a CPU stall.

The DSP includes many other peripherals; among them, two counter-timers, TIMER1 and TIMER2 [15]. They are broadly configurable through a configuration register. The input can be connected to the system clock or to an external pin, driven by a CMOS signal, thus selecting if the device is acting as a counter of external events or as a timer. The count register can be read and used by the program. Based on the counts and the value of a period register, an output is driven, in order to generate square waves of different duty cycle. Moreover, the

output can drive an interrupt. We used TIMER1 as a counter of external events. In this way, the input of the spectrum analyzer can be driven by a discrete pulse train, as in the application to DLS discussed below, where the timer is connected to the output of a photon counting photomultiplier. Alternatively, by using a voltage to frequency converter, the input of the timer could be driven by an analog signal, such as the one from a photodiode. The other timer, TIMER2, generates a periodic interrupt, in order to define the integration period: the interrupt service routine reads the counts of TIMER1 and resets it, passing the number of counts to the processing program.

Texas Instruments provides a DSK (DSP Starter Kit), including a board with the DSP and some peripherals; among them, a device that allows to connect the board to a PC through a parallel port. The PC can read and write the memory of the DSP, without halting the CPU, and can run a program. The PC uploads the program that evaluates the power spectrum of the signal in the SRAM, then runs it, and periodically reads the results.

The software consists of two parts, one for the DSP and one for the host computer. Texas Instruments provides Code Composer Studio (CCS), that includes a C compiler and an assembler for the DSP. The program for the DSP has been written in assembler code, since in this way a high processing speed is obtained in conjunction with an accurate timing. Moreover, the provided software includes some libraries for building host programs that interact with the DSP, that is, to upload a program, run it, and read some memory locations in the DSP [16]. All the software we developed is freely available. [17]

IV. DISCRETE WAVELET TRANSFORM PROGRAM

With respect to the hardware correlators traditionally used within the Dynamic Light Scattering community, the use of a DSP allows the flexible implementation of many processing algorithms simply by dowloading a different processing code onto the board. These algorithms include FIR and IIR filters, cross correlation, convolution filters etc.

In this section, we discuss the implementation of the discrete, real time wavelet algorithm on the DSK board.

The overall data structure is shown in Fig. 1, along with a simplified description of the data flow. The higest sampling frequency is about 0.3MHz and the lowest frequency corresponds to a period of some hours. Every frequency octave represents a level in the wavelet processing algorithm. Figure 1 shows only levels 0 and 1 and part of level 2. The entire structure is made up by $N = 32$ levels, each corresponding to a measured frequency. Every level contains a circular queue y_j^k of double precision floating points to store the last M values of the coarse grained signal, where M is the length of the MW. The N queues are managed by using the circular addressing mode of the DSP; this allows only values of M that are powers of two. Therefore, the Daubechies wavelets our program can use are those with length $M = 4$, 8, 16, 32 and 64. We will discuss the implementation of the Daub4 $M = 4$ transform.

Level 0 is driven by TIMER1, configured as a counter, which counts the digitized pulses at the input of the spectrum analyzer within a selected bin. The integration time is defined by TIMER2, configured as a timer, so that its output signal generates an interrupt at $f_s = 375$KHz, corresponding to the sampling frequency. At each sampling time the number of pulses counted by TIMER1 is fed to the first element of the shift register y_n^0 in Level 0 and the other cells are shifted down. Every two sample times the content of the shift register is convolved with the two wavelet coefficient banks g_n and h_n, the MW and the smoothing filter coefficients respectively. The result of the convolution with the bank h_n feeds the shift register y_n^1 in Level 1 and gives rise to a coarse grained replica of the signal at half the sampling frequency. The in-quadrature component obtained from the convolution with bank g_n contains the wavelet coefficients c_n^0 which specify the local amplitude of the band-pass filtered signal in the frequency range $(\omega_0/2, \omega_0)$, where $\omega_0 = \pi f_s$. The process is repeated in cascade for all the levels.

The processing of N levels requires to store additional informations: the sum and the counter needed to evaluate the mean of $\left|c_n^k\right|^2$, the current address inside the queue and the status of the queue.

The coefficients c_n^k feed the register $\sum \left|c_n^k\right|^2$, which stores the mean square amplitude of the high-pass filtered signal representing the power spectrum $S(\omega)$ in the angular frequency range $\left(\omega_0/2^{k+1}, \omega_0/2^k\right)$.

The status of the queue can be 0 (the queue has just been processed), 1 (the queue had one input) or 2 (the queue is full and requires processing); it is incremented by one each time an element is put in the queue and is reset to zero when it is processed. At the initialization, the status is set to $-M + 2$, so that the queue is filled at least with M elements before it is processed the first time.

As outlined above, Level 1 is updated only when two new samplings are available in Level 0. Therefore the update of Level 1 occurs with a frequency $f_s/2$, and its processing with a frequency $f_s/4$, which corresponds to the update frequency of Level 2, and in general Level k is updated at a frequency $f_s/2^k$ and processed at $f_s/2^{k+1}$. The sum of all the processing frequencies for every queue, $\sum_n f_s/2^{k+1}$, converges to f_s as $N \to +\infty$. This means that the frequency at which all the queues are processed is smaller than the sampling frequency f_s. At each sampling time, our algorithm processes the lowest-level full queue, if any. This ensures that, by processing exactly one queue at each sampling time, the output values y_n^k never go to an already full queue. For the Daubechies wavelets with $M = 4$ all the operations can be performed in about 2μs.

Beyond the processing sofware on the DSP board two

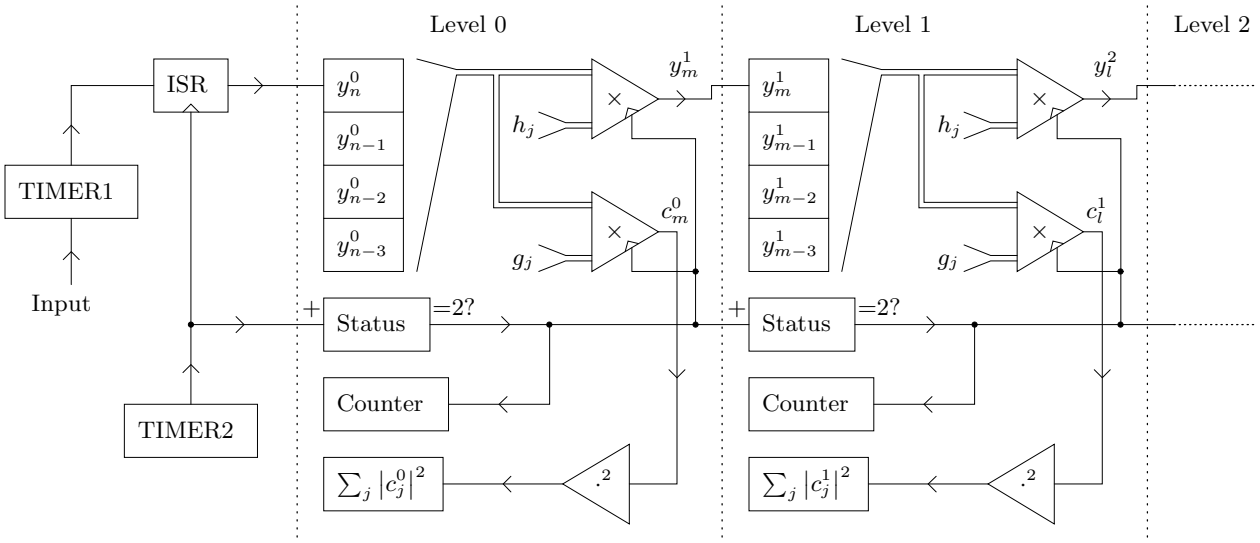

FIG. 1: Data structure and data flow of the wavelet transform spectrum analyzer.

host programs run on the host computer: the first uploads the DSP programs and runs it; the second reads the memory of the DSP, without halting the CPU. This program is used to get a real time display of the processed spectrum. The read program accesses the DSP memory through the parallel port. Inside the DSK board, data are read from memory by using a low priority DMA channel, and thus without interfering with the CPU operations.

Another processing method, not yet implemented, involves the processing of the cross spectrum of two signals. This is very useful to get rid of noise sources such as afterpulsing from a photomultiplier detector. This method involves the parallel use of two processing structures like the one shown in Fig. 1. Each detector signal feeds one of the TIMER input. The output of each structure is a set of wavelet coefficients c^k_{an} and c^k_{bn}. The averaged product of the coefficients $\sum c^k_{an} c^k_{bn}$ gives the desired cross spectrum. Due to the simultaneous operation of two processing structures, the minimum sampling frequency is reduced by a factor of two.

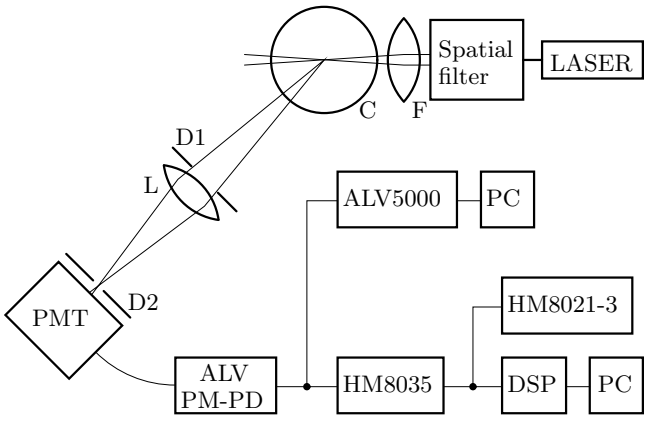

FIG. 2: Diagram of the experimental setup.

V. EXPERIMENTAL RESULTS

To assess the performances of the Spectrum Analyzer we have performed test measurements on a colloidal suspension and on a model system giving rise to a power-law power spectrum.

The experimental setup is based on the traditional DLS one. A diagram of the setup is shown in Fig. 2. The beam coming from a JDS Uniphase 35mW CW HeNe LASER model 1145P is spatially filtered and focused by the lens F at the center of the sample contained in the cuvette C. Light scattered from the sample is collected by the lens L and by the diaphragms D1 and D2. The scattered radiation eventually impinges onto the photocathode of a EMI 9863 B04/350 photon counting Photomultiplier Tube (PMT). The scattering angle can be changed by rotating the collecting optics and the PMT around the cuvette by means of a goniometer. The current pulses from the PMT are amplified and filtered by an ALV PM-PD preamplifier-discriminator, which also digitizes the pulse train at TTL levels. In the traditional DLS apparatus the signal is then fed to an ALV5000 multi tau hardware correlator hosted in a personal computer. Alternatively, the digitized signal at the output of the amplifier-discriminator can be routed to a timer input of the DSP board, which is connected to a personal computer for the configuration and visualization of measurements. The DSP board is also connected to a HAMEG 1.6 GHz frequency counter model HM8021-3 and a HAMEG 20 MHz pulse generator model HM8035 for testing purposes.

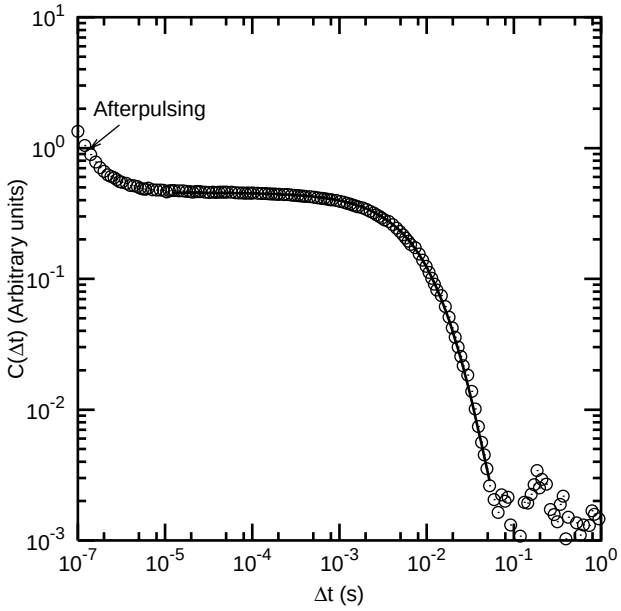

FIG. 3: Correlation function of the intensity fluctuations of light scattered at 30° by a colloidal suspension, in the Dynamic Light Scattering regime, measured with ALV equipement. Circles represent the experimental data. The continuous line represents a fit of the experimental data up to the second cumulant.

A. Colloidal suspensions

The test on the colloidal suspension were performed on calibrated polystyrene latex of 0.115μm diameter, diluted at a volume fraction of about $\phi = 1.5 \times 10^{-6}$. For a dilute suspension of monodisperse brownian particles the Homodyne time autocorrelation function of the intensity fluctuations in the scattered light has the usual exponential form $C(t) = \langle I \rangle^2 [1 + A \exp(-\Gamma t)]$, where $\Gamma = 2Dq^2$ and $D = k_B T/(6\pi\eta a)$ is the Stokes-Einstein Diffusion coefficient, η is the shear viscosity for the solvent and a the particle radius. The correlation function measured at a scattering angle of 30° is plotted in Fig. 3 as a function of the lag time. The experimental data show the decay of the correlation function within a dynamic range of about 2.5 decades. The run duration was 2700s.

At the longer delay times the correlation function is dominated by noise due to the poor statistical sample accumulated. The additional contribution at small lag times is due to the afterpulsing of the PMT. The afterpulses of the PMT used to performed the measurement have a characteristic range of correlation times between 0.1μs and 3.2μs, which give rise to a stretched exponential decay at small lags. The decay at lags larger than about 3.2μs is determined by the intensity fluctuations due to the brownian motion of the colloid. Data can be fit with an exponential function $\exp(-\Gamma t)$. A more refined analisys of the experimental data involves the inclusion of polidispersity effects in the fitting procedure. This is traditionally performed by a cumulant analisys of the correlation function [8]. In the case of a small polidispersity the correlation function up to the second cumulant is given by

$$C(t) \propto \exp\left(-\Gamma_0 |t| + \frac{1}{2}\sigma^2 t^2\right) \propto \int \exp(-\Gamma |t|) \exp\left[-\frac{(\Gamma - \Gamma_0)^2}{2\sigma^2}\right] d\Gamma, \quad (3)$$

where the second equality shows that polidispersity effects give rise to the superposition of exponential decays centered around a central linewidth Γ_0, these decays being weighted by a gaussian function with variance σ representing the polidispersity. The best fit of the experimental data with Eq. (3) is indicated by the solid line in Fig. 3 and yields $\Gamma_0 = 140$Hz and $\sigma = 42$Hz.

We performed the same experiment, by using the DSP WTSA and the same homodyne detection scheme outlined above. According to the Wiener-Kintchine theorem, the power spectrum of the fluctuations in the intensity of light scattered by the colloidal suspension is the Fourier transform of the correlation function $C(t)$. For diluted monodisperse brownian particle the power spectrum has a Lorenzian shape: $S(\omega) \propto \Gamma/\left(\Gamma^2 + \omega^2\right)$.

Figure 4 shows data for the measured power spectrum as a function of angular frequency ω. Raw data are represented with crosses. At the smaller frequency the effect of noise due to the reduced statistical sample is evident. This occurs at angular frequencies roughly smaller than 1rad/s, corresponding to a time delay of the order of 6s. However, this same noise affects the correlation function shown in Fig 3 starting from about $t = 10^{-1}$s. As the duration of the experiment is in both cases 2700s, the wavelet processing allows a better convergence at larger delay times: the timescale range across which the power spectrum can be reliably determined is roughly two decades more extended than that of the correlator. At larger frequency the power spectrum in Fig. 4 falls down up to a constant base line, represented by a horizontal dashed line. This baseline is determined by the shot noise. In fact, it is well known that the detection of photons is a random process characterized by a Poisson distribution and gives rise to a delta-correlated white noise, whose power spectrum corresponds to the average

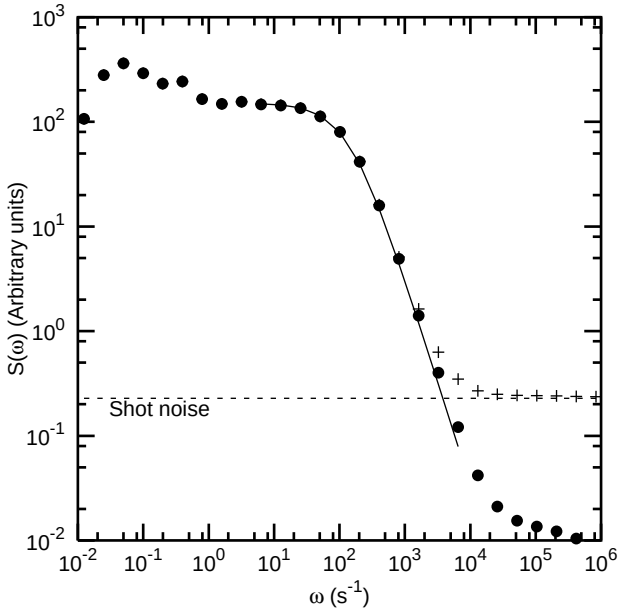

FIG. 4: Power spectrum of the intensity fluctuations of light scattered at 30° by a colloidal suspension, in the Dynamic Light Scattering regime, measured with WTSA. Crosses represent the raw data. The dashed line is the baseline due to the shot noise. Circles represent the power spectrum obtained by subtracting the baseline from the raw data. The continuous line is the best fit of the experimental data up to the second cumulant.

number of photons detected within the sampling time [8].

$$C(t) \propto \frac{\langle I(t')\, I(t'+t)\rangle}{\langle I^2(0)\rangle} - 1 + \langle n\rangle\, \delta(t)\,. \qquad (4)$$

In the frequency space this gives rise to a constant term $\langle n\rangle$, represented by the dashed line in Fig. 4, which adds up to the power spectrum. The average number of photons $\langle n\rangle$ can be easily processed in real time and subtracted.

The circles in Fig. 4 show experimental data for the power spectrum after the subtraction of the shot noise contribution. The data span a dynamic range of more than 4 decades. Data can be represented by a Lorenzian curve $\Gamma/\left(\omega^2+\Gamma^2\right)$. In this case also, a more refined analisys involves the inclusion of polidispersity effects. By taking the Fourier transform of Eq. (3) we get:

$$S(\omega) \propto \int \frac{\Gamma}{\omega^2+\Gamma^2} \exp\left[-\frac{(\Gamma-\Gamma_0)^2}{2\sigma^2}\right] \mathrm{d}\Gamma. \qquad (5)$$

Therefore the power spectrum is the superposition of lorenzians weighted by the same gaussian function introduced to describe the polidispersity in the correlation analysis. We evaluated numerically the integral of Eq. (5), in order to fit the results in Fig. 4. However, each circle in Fig. 4 represents the integral of the power spectrum across an octave; this smooths even more the bell-shaped measured curve; this effect has been considered in the fit procedure. We obtained the best fit with $\Gamma_0 = 158$Hz and $\sigma = 37$Hz, which favourably compare with the results obtained with the correlator. The best fitting curve is represented by the solid line.

At the higher frequencies the spectrum is dominated by the contribution of afterpulses to the intensity fluctuations which give rise to the tail in the range $10^4 - 10^6$Hz in Fig. 4.

The wavelet analysis of the data presents some advantages when compared to correlation techniques. A notable advantage is represented by the way background subtraction is achieved. In correlation techniques a constant baseline has to be subtracted from the measured correlation function to recover data like those shown in Fig. 3. The baseline represents the correlation function at large la times, where correlations disappear. The intrinsic contrast of the correlation function, defined by the ratio between the amplitude of the completely correlated part at $t = 0$ and the uncorrelated part at large lag times, $[C(0) - C(+\infty)]/C(\infty)$, cannot exceed the value of two. Therefore, the signal and the background are of the same order of magnitude and the dynamic range is strongly limited by the accuracy in the baseline. The accuracy in the baseline can be determined from the arguments presented in Ref. [18] and summarized below. Let us call τ_L the largest decay time in the correlation function and T the duration of the run. Samples acquired at time lags smaller than τ_L are correlated, therefore the number of independent samples acquired during T is $N_c = T/\tau_L$. This independent samples average out according to a normal distribution to give rise to the baseline. Therefore, the accuracy in the baseline is of the order of $1/N_c^{1/2}$. In the case of the results presented in Fig. 3, $\tau_L = 40$ms, $T = 2700$s, thus giving $1/N_c^{1/2} = 4\times10^{-3}$, which corresponds fairly well to the dynamic range of about 2.5 decades of the measurement. The same argument can be applied to the accuracy of the baseline in the power spectrum determined with the WTSA and presented in Fig. 4. In this case, however, the baseline is generated by the shot noise, which is correlated on a time of the order of the inverse of the sampling frequency ω_0. The number N of independent samples corresponds to the total number of samples accumulated at ω_0. For the results presented in Fig. 4 $N = 10^9$ and the accuracy of the baseline is of the order

of $1/N^{1/2} = 3 \times 10^{-5}$. By eliminating the contribution of afterpulsing to the spectrum as described in Sect. IV, the dynamic range could potentially be extended about five decades above the intrinsic contrast of the measurement, which in this case amounts to about 10^3. It has to be remarked that in this case there's no upper limit for the contrast, therefore a dynamic range as high as 10^{10} could potentially be obtained.

B. Model system

The ultimate task of the WTSA is the characterization of signals characterized by a wide distribution of timescales.

To assess its performances we have chosen a simple model system made up by strongly diluted diffusing brownian particles illuminated by a wide collimated laser beam. This system gives rise to a nice power-law power spectrum with the exponent $-3/2$. A detailed derivation of the predicted power spectrum is presented in Appendix. The sample is a colloidal suspension of polystyrene latex spheres of 10μm diameter, suspended in water at a concentration of roughly 10^4particles/cm^3. The solvent is a mixture of equal volumes of water and deuterated water, so that its density is matched to that of the colloid within 0.1%. The sample is illuminated by a gaussian laser beam with a diameter at $1/e^2$ of about 1mm. The scattering volume is delimited by two slits perpendicular to the beam. Therefore the scattering volume is determined in one direction by the hard edge of the slits and in the other direction by the gaussian profile of the beam. The scattered light is collected at 90° with respect to the main beam.

Due to the strongly diluted sample and to the wide beam illumination, fluctuations in the intensity of the scattered light are mostly determined by changes in the number of particles in the scattering volume. By using a wide laser beam, the coherence areas onto the photocatode of the PMT are very small. Therefore, the photocatode collects the averaged contribution coming from many coherence areas. In this way the component of the correlation function due to the diffusion of particles has a vanishingly small contrast, when compared to the averaged intensity measured by the photodetector. The signal onto the PMT thereby represents the superposition of the intensities scattered by single particles. As it is shown in the Appendix, intensity fluctuations spanning a wide frequency range are excited when particles cross the hard edge at the boundary of the scattering volume.

Figure 5 shows the correlation function of the fluctuations in the scattered intensity. The correlation function shows an almost featureless structure and a narrow dynamic range. The correlation function is almost flat within about six decades in lag time, due to the long tails associated with the slowest modes. The peak at small lags still represents the contribution of afterpulses. The correlation function eventually decays at times of the order of 60s. However, this decay is an artifact due to the finite measurement time. In fact, correlation analysis assumes that the correlation function decays to zero at large delays, once its baseline has been subtracted. The baseline is usually evaluated from the value of the correlation function at very large delays. However, for time-scale invariant processes, the baseline still contains the contribution of the slowest modes. Therefore, an increase of the acquisition time involves a decay at a larger time. As a rule of thumb, experimental data for the correlation function are reliable up to delays roughly 100 times smaller than the acquisition time. This is a feature of correlation techniques which strongly limits their ability in characterizing processes where an upper time scale is absent.

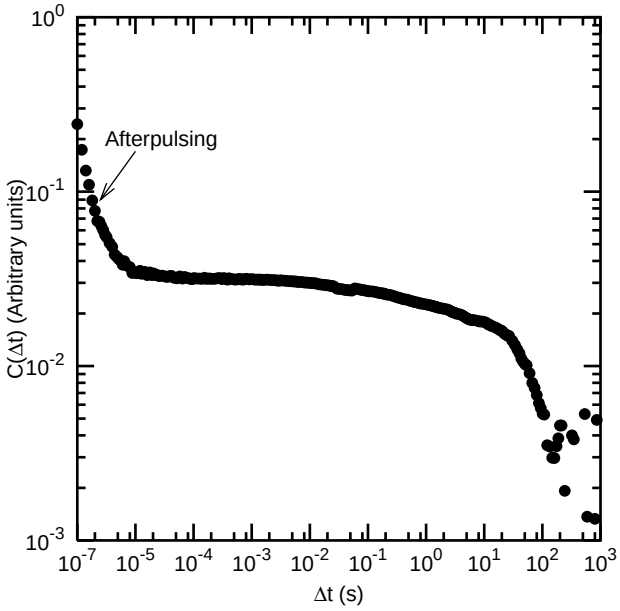

FIG. 5: Correlation function of the intensity fluctuations in the model system, measured with ALV equipement.

Figure 6 shows the power spectrum of the fluctuations measured by means of the WTSA. The crosses represent the raw data, the horizontal line the background level due to shot noise and the circles the subtracted data representing the power spectrum. The most prominent feature of the results in Fig. 6 is the impressive dynamic

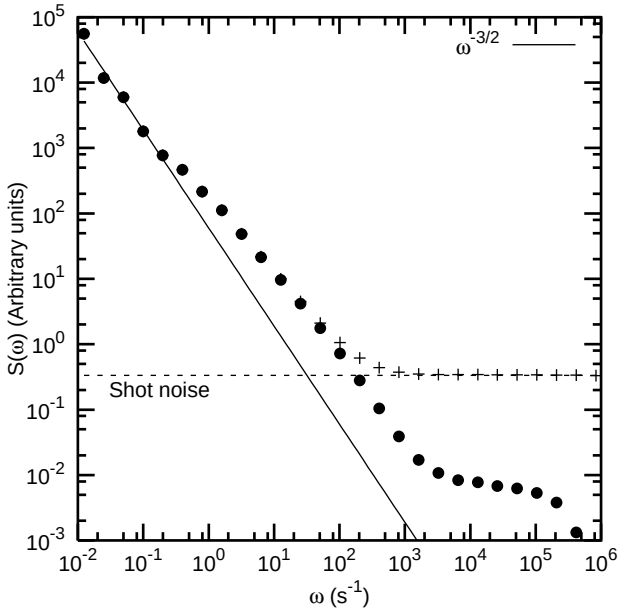

FIG. 6: Power spectrum of the intensity fluctuations in the model system, measured with WTSA. Crosses represent the raw data. The dashed line is the baseline due to the shot noise. Circles represent the power spectrum obtained by subtracting the baseline from the raw data. The continuous line represents a power-law with exponent $-3/2$ for comparison.

range spanning about 8 decades. The measured power spectrum decays approximately as a power law with an exponent of the order of -1.2. The straight line represents a power law with exponent $-3/2$ for comparison. At the larger frequency, the contribution of afterpulses is apparent.

Deviations from the power law behavior at intermediate frequencies can be attributed to a residual contribution of the diffusion of particles to the correlation function. Such a contribution cannot be completely eliminated, even by collecting a large number of coherence areas onto the multiplier. As outlined above, the diffusion of particles gives rise to fluctuations in the scattered intensity at 90°, characterized by lorentzian spectrum with a linewidth of the order of $\Gamma = 20$Hz. Deviations form the power-law behavior occur at frequencies roughly centered around Γ. However, a more refined analysis of the data, including the evaluation of contributions due to diffusion and due to number fluctuations to the spectrum, is beyond the aim of this paper.

The wavelet transform analysis is particularly effective for processes where the power law exponent α is larger than 1, like the model system just described. In fact, correlation techniques completely fail when applied to such systems. For exponents smaller than one the spectral behavior can be characterized either by measuring the power spectrum $S(\omega) \propto 1/\omega^{\alpha}$ or by measuring the correlation function, which also exhibits a power-law behavior $C(t) \propto t^{1-\alpha}$. In the limit $\alpha \to 1$ the correlation function becomes flat. For $\alpha > 1$ the correlation function is still flat and time independent. Naively speaking, this is due to the strong divergence of the power spectrum at small frequency which behaves as a delta shaped spectrum. The diverging energy of the small frequency modes gets uniformly distributed along the lag time axis of the correlation function, which becomes flat. More rigorously, the correlation function can be obtained by Fourier transforming the power-law spectrum, regularized to avoid its divergence at $\omega = 0$:

$$C(t) \propto \int \lim_{\epsilon \to 0} \frac{1}{\epsilon + \omega^{\alpha}} \exp(-i\omega t) \mathrm{d}\omega. \qquad (6)$$

For $\alpha > 1$, the spectrum has an integrable power law tail for $\omega \to +\infty$. It approximates a delta function $\delta(\omega)$ as $\epsilon \to 0$. Therefore, for $\alpha \geq 1$, $C(t)$ is a constant: a correlation function like that shown in Fig. 3 is completely featureless and useless.

An important application of the WTSA is the time dependent analisys of transient behavior during processes such as gelation [6, 19] and colloidal aggregation [20]. In general, during such transients the highest frequencies are excited at first, and lower frequencies get gradually excited as time goes by. This introduces a characteristic lag time τ_c marking the boundary between excited and non-excited modes. The proper characterization of this processes involves the measurement of the power spectrum (or correlation function) from data sampled along a duration time T larger then τ_c, so to be able to resolve τ_c. In principle a longer T allows to measure the power spectrum or correlation function with a higher accuracy, due to the increase of the number of independent sample processed. However the lag time τ_c changes during the transient. Therefore, a compromise has to be reached between the need to keep T not much larger than τ_c and the desire to measure the spectrum with a high accuracy.

As far as the WTSA is concerned, the same argument used to estimate the accuracy of the baseline can be used to get an order of magnitude estimate of the number of samplings needed to get a chosen accuracy. Suppose that we want to obtain the power spectrum at a frequency ω_k with an accuracy better than a. As it was shown in section II, the power spectrum is calculated by averaging the squared wavelet coefficients: $S(\omega_k) \propto \sum_n \left|c_n^k\right|^2$. We recall here that the coefficients c_n^k represent the wavelet coefficients evaluated at subsequent times n. Although this argument is not rigorous, for a generic random sig-

nal, it is reasonable to assume that the coefficients evaluated at different times are independent. Therefore the percentual error on $S(\omega_k)$ scales as $1/N_k^{1/2}$, where N_k is the number of samplings of the signal accumulated at the frequency ω_k. In this way, a 1% in $S(\omega_k)$ is achieved by sampling the signal up to frequencies of the order of $10000\omega_k$. However, an order of magnitude estimate of the power spectrum can be obtained from a few samplings at ω_k.

Therefore, a very important feature of the wavelet analysis, when compared to correlation techniques, is its ability to characterize the power spectrum at small frequencies, without introducing artifacts related to the finite acquisition time. This can be appreciated from Fig. 6, where the smallest experimental angular frequency is of the order of 10^{-2}Hz, roughly corresponding to the acquisition time of 2700s. The wavelet analysis only yields an order of magnitude estimate of the amplitude of this mode, due to the absence of a significative statistical sample. However, the wide dynamic range involved in the power spectrum makes it almost insensitive to background subtraction at small frequencies, so that no characteristic times associate with the duration of the experiment are introduced in the subtraction. Therefore, when compared with correlation techniques, wavelet analysis allows a dramatic increase of the investigated frequency range, this increase amounting to almost two decades. This feature makes the WTSA the ideal tool to investigate slow processes, non-stationary processes, time-scale invariant processes and processes characterized by a wide distribution of time-scales in general.

Acknowledgments

We thank Texas Instruments DSP University program for the gift of the DSK board and for technical support. We also thank M. Giglio for discussion and support.

APPENDIX A: POWER SPECTRUM OF THE NUMBER FLUCTUATIONS OF BROWNIAN PARTICLES IN A GIVEN VOLUME.

In this appendix we will derive the power spectrum determined by the number fluctuations of brownian particles diffusing within a scattering volume delimited by sharp edges on two sides and by the gaussian profile of a beam on the two perpendicular sides. We will assume that the sample is illuminated by a wide collimated beam, so that spatial coherence effects can be neglected. Some of the arguments we use in the following are also used in the derivation of fluorescence correlation spectroscopy. [8]

Given N particles, at position $\vec{x}_n$, the measured intensity I_t at time t is the sum of the intensities scattered by each particle, since light is collected over several speckles, and interference plays no role. Moreover, the intensity scattered by each particle is proportional to the intensity $I(\vec{x})$ of the main beam at the position of the particle:

$$I_t \propto \sum_{n=0}^{N-1} I\left[\vec{x}_n(t)\right]. \tag{A1}$$

Roughly speaking, I_t is proportional to the number of particles inside the main beam, weighted by the intensity in that point. The temporal correlation function is thus:

$$C_I(\tau) = \langle I_t I_{t+\tau}\rangle \propto \sum_{n,m=0}^{N-1} \left\langle I\left[\vec{x}_n(t)\right] I\left[\vec{x}_m(t+\tau)\right]\right\rangle, \tag{A2}$$

where the brackets represent the average over t. By assuming that the particles are non-interacting, their positions are not correlated:

$$C_I(\tau) \propto N(N-1)\bar{I}^2 + N\left\langle I\left[\vec{x}(t)\right] I\left[\vec{x}(t+\tau)\right]\right\rangle, \tag{A3}$$

where the bar represents the average over the volume V of the whole cell. From this equation, we derive the relative mean square value of the fluctuations of I_t:

$$\frac{\left\langle I_t^2\right\rangle - \langle I_t\rangle^2}{\langle I_t\rangle^2} = \frac{C_I(0) - C_I(+\infty)}{C_I(+\infty)} = \frac{1}{N}\frac{\bar{I^2} - \bar{I}^2}{\bar{I}^2}. \tag{A4}$$

Roughly speaking, $\left(\bar{I^2} - \bar{I}^2\right)/\bar{I}^2$ is the ratio V/V_b, where V_b is the volume inside the main beam. This statement can be easily proved for an hypotetic beam with constant intensity inside V_b, vanishing outside. By calling N_b the number of particles inside the beam:

$$\frac{\left\langle I_t^2\right\rangle - \langle I_t\rangle^2}{\langle I_t\rangle^2} = \frac{1}{N_b}. \tag{A5}$$

This equation is analogous to the relation between number fluctuation and mean number for Poisson distribution. In order for the fluctuations to be strong, only a few particles must be inside the beam simultaneously.

The diffusion of each particle can be described as a random walk; $P_\tau(\vec{y} - \vec{x})$, the probability that a particle in $\vec{x}$ goes in $\vec{y}$ in a time τ, is thus:

$$P_\tau(\Delta\vec{x}) = \frac{1}{\left[\sqrt{2\pi}\sigma(\tau)\right]^3} e^{-\frac{\Delta\vec{x}^2}{2\sigma^2(\tau)}}, \tag{A6}$$

where $\sigma(\tau) = \sqrt{D|\tau|}$ and D is the diffusion coefficient. By using this probability distribution, we can explicitly rewrite Eq. (A3):

$$C_I(\tau) \propto c + \int I(\vec{x})\, I(\vec{y})\, P_\tau(\vec{y} - \vec{x})\, \mathrm{d}\vec{x}\mathrm{d}\vec{y}, \tag{A7}$$

where c is a constant. The convolution operator is diagonalized by Fourier transform:

$$C_I(\tau) = c + \int \left|I(\vec{q})\right|^2 P_\tau(\vec{q})\, \mathrm{d}\vec{q}, \tag{A8}$$

where $P_\tau(\vec{q})$ and $I(\vec{q})$ are the Fourier transforms in $\vec{x}$ of $P_\tau(\vec{x})$ and $I(\vec{x})$:

$$P_\tau(\vec{q}) = e^{-\frac{1}{2}q^2\sigma^2(\tau)}. \quad \text{(A9)}$$

By Fourier transforming Eq. (A8) in τ:

$$S_I(\omega) = \int |I(\vec{q})|^2 P_\omega(\vec{q})\,\mathrm{d}\vec{q}, \quad \text{(A10)}$$

where $P_\omega(\vec{q})$ is the Fourier transform in τ of $P_\tau(\vec{q})$ as defined by Eq. (A9):

$$P_\omega(\vec{q}) = \frac{1}{\pi}\frac{Dq^2}{\omega^2 + D^2q^4}. \quad \text{(A11)}$$

Now, we explicitly give the intensity distribution $I(\vec{x})$ within the scattering volume:

$$I(x,y,z) = I_0\chi_{[-L/2,L/2]}(z)\,e^{-\frac{x^2+y^2}{2R^2}}, \quad \text{(A12)}$$

where L is the length of the portion of the beam we observe, R is the radius of the main beam at $e^{-1/2}$ and I_0 is the intensity at the center of the main beam. The Fourier transform is:

$$I(q_x,q_y,q_z) = \frac{4\pi I_0}{Q_L Q_R^2}\frac{\sin(q_z/Q_L)}{q_z/Q_L}e^{-\frac{q_x^2+q_y^2}{2Q_R^2}}, \quad \text{(A13)}$$

where $Q_L = 2/L$ e $Q_R = 1/R$. By inserting the explicit expressions of Eq. (A9) and Eq. (A13) in Eq. (A10):

$$S_I(\omega) = \frac{16\pi I_0^2}{Q_L^2 Q_R^4}\int \frac{\sin^2(q_z/Q_L)}{(q_z/Q_L)^2}e^{-\frac{q_x^2+q_y^2}{Q_R^2}} \times \frac{D\left(q_x^2+q_y^2+q_z^2\right)}{\omega^2 + D^2\left(q_x^2+q_y^2+q_z^2\right)^2}\mathrm{d}q_x\mathrm{d}q_y\mathrm{d}q_z. \quad \text{(A14)}$$

Now, we impose that $\omega \gg DQ_R^2$ and $\omega \gg DQ_L^2$. This means that ω corresponds to times much shorter than the time needed by a particle to travel across the main beam. Under this condition, we can neglect q_x and q_y at the denominator, since the gaussian part in the integrand imposes $|q_x| \lesssim Q_R$ and $|q_y| \lesssim Q_R$; then, we integrate over q_x and q_y:

$$S_I(\omega) = \frac{16\pi I_0^2}{Q_L^2 Q_R^2}\int \frac{\sin^2(q_z/Q_L)}{(q_z/Q_L)^2}\frac{D\left(q_z^2+2Q_R^2\right)}{\omega^2 + D^2q_z^4}\mathrm{d}q_z. \quad \text{(A15)}$$

The $\sin^2(q_z/Q_L)$ has fast oscillations, and averages to $1/2$ for $q_z \gg Q_L$:

$$S_I(\omega) = \frac{8\pi I_0^2}{Q_R^2}\int \frac{Q_L^2}{q_z^2+Q_L^2}\frac{D\left(q_z^2+2Q_R^2\right)}{\omega^2 + D^2q_z^4}\mathrm{d}q_z. \quad \text{(A16)}$$

The leading term in the integral is the q_z^{-2} coming from the sinc function. This means that the behaviour of the measured intensity is mainly due to particles crossing the sharp edges of the slits, moving along the main beam, while the movements inside and outside the beam can be neglected.

Since Q_R and Q_L are of the same order of magnitude:

$$S_I(\omega) = 8\pi I_0^2 D\int \frac{1}{\omega^2 + D^2q_z^4}\mathrm{d}q_z. \quad \text{(A17)}$$

The integral converges; by substituting $q_z = x\sqrt{\omega}$:

$$S_I(\omega) \propto \omega^{-3/2}. \quad \text{(A18)}$$

[1] Wentian Li, One - over - f noise, http://linkage.rockefeller.edu/wli/1fnoise/ : represents an extensive bibliographic resource about $1/f$ noise.

[2] D. Sornette, *Critical phenomena in natural sciences*, Springer series in synergetics, Springer, Berlin, 2000.

[3] J. P. Sethna, K. A. Dahmen, and C. R. Myers, Nature **410**, 242 (2001).

[4] R. N. Mantegna and H. E. Stanley, *Introduction to Econophysics*, Cambridge University Press, Cambridge, 2000.

[5] M. Le Bellac, *Des phénomènes critique aux champs de jauge*, InterEditions, Paris, 1988.

[6] M. Kroon, G. H. Wegdam, and R. Sprik, Europhys. Lett. **35**, 621 (1996).

[7] R. Sprik and E. Baaij, Rev. Sci. Instrum. **73**, 2440 (2002).

[8] B. J. Berne and R. Pecora, *Dynamic Light Scattering*, Wiley, New York, 1976.

[9] R. Pecora, editor, *Dynamic Light Scattering*, Plenum Press, New York, 1985.

[10] W. Brown, editor, *Dynamic light scattering*, Clarendon Press, Oxford, 1993.

[11] L. Cipelletti, S. Manley, R. C. Ball, and D. A. Weitz, Phys. Rev. Lett. **84**, 2275 (2000).

[12] L. Ramos and L. Cipelletti, Phys. Rev. Lett. **87**, 245503 (2001).

[13] W. H. Press, S. A. Teukolsky, W. T. Vetterling, and B. P. Flannery, *Numerical recipes*, Cambridge University Press, Cambridge, 1994.

[14] Texas Instruments, *TMS320C6000 CPU and Instruction Set Reference Guide*, 2000, Available at http://www.ti.com/sc/docs/psheets/man_dsp.htm as

SPRU189.
[15] Texas Instruments, *TMS320C6000 Peripherals Reference Guide*, 2001, Available at http://www.ti.com/sc/docs/psheets/man_dsp.htm as SPRU190.
[16] Texas Instruments, *TMS320C6000 Programmer's Guide*, 2001, Available at http://www.ti.com/sc/docs/psheets/man_dsp.htm as SPRU198.
[17] http://www.mi.infn.it/labgiglio/WTSA.htm.
[18] V. D. Giorgio and J. B. Lastovka, Phys. Rev. A **4**, 2033 (1971).
[19] M. Kroon, G. H. Wegdam, and R. Sprik, Phys. Rev. E **54**, 6541 (1996).
[20] A. Vailati, D. Asnaghi, M. Giglio, and R. Piazza, Phys. Rev. E **48**, R2358 (1993).